Hindawi
Adsorption Science & Technology
Volume 2022, Article ID 8237403, 18 pages
https://doi.org/10.1155/2022/8237403

Research Article

A New Schiff Base Organically Modified Silica Aerogel-Like Material for Metal Ion Adsorption with Ni Selectivity

João P. Vareda,[1] **Paulo D. Matos**,[1] **Artur J. M. Valente**,[2] **and Luisa Durães**[1]

[1]*University of Coimbra, CIEPQPF, Department of Chemical Engineering, Rua Sílvio Lima, 3030-790 Coimbra, Portugal*
[2]*University of Coimbra, CQC, Department of Chemistry, Rua Larga, 3004-535 Coimbra, Portugal*

Correspondence should be addressed to João P. Vareda; jvareda@eq.uc.pt and Luisa Durães; luisa@eq.uc.pt

Received 25 October 2021; Revised 10 February 2022; Accepted 18 February 2022; Published 9 March 2022

Academic Editor: Chinenye Adaobi Igwegbe

Nickel has several industrial uses and is a valuable metal, making its selective separation and recycling a priority goal. A novel adsorbent, a Schiff base organically modified silica (ORMOSIL) aerogel, was prepared, for selective nickel removal from wastewater with other metal ions, by including a salen ionophore in the silica-based network. The newly developed adsorbent takes advantage of the salen's selectivity and of the high porosity of silica aerogels. The aerogel-like adsorbent was prepared via sol-gel chemistry, using a coprecursor approach and ambient pressure drying. The inclusion of the Schiff base in the silica network was accomplished by reacting an amine-containing silica precursor with an aldehyde and confirmed by nuclear magnetic resonance (NMR) analysis. The adsorbent shrunk only 10% after evaporative drying, which resulted in a highly porous material (85% porosity, 4 $cm^3 g^{-1}$ specific pore volume). The low surface area of 28 m^2 g^{-1} was due to the predominantly macroporous structure of the material (mean pore diameter of 563 nm). Adsorption isotherms and kinetic curves with single and binary mixtures of cations at room temperature were used to assess the selectivity of the adsorbent. The adsorption follows a BET (Brunauer-Emmett-Teller) trend. Due to the proximity of the oxygen and nitrogen atoms in the salen and steric hindrance from their neighboring atoms, it is likely that only the smallest hydrated cations can act as a coordination center and interact with both donor atoms. Thus, nickel was fairly removed (50 mg g^{-1}), while other cations barely interacted with the adsorbent (cadmium adsorption maximum of 5 mg g^{-1}). The estimated selectivity coefficient for nickel ranges from 1.8, in relation to copper, to 9.4 relatively to cadmium, which can be relevant for the separation of nickel in several industrial contexts, for instance, from electroplating sludge.

1. Introduction

Heavy metals (HMs) are pollutants that accumulate in the environment, and due to high emissions from human activities, create severe levels of pollution in water courses, sediments, and soils [1, 2]. They are mobile hence leach and are absorbed by organisms, further spreading through ecosystems [3–7]. This issue can be overcome by stopping the pollutant emissions and/or deploying advanced waste treatment techniques. Moreover, many heavy metals are used as raw materials in different industries [8, 9] and have commercial value [9, 10]. Among them, we can cite copper, lead, cadmium, and nickel. They feature high toxicity and are prone to human-made emissions and accumulation in the environment, and concomitantly, they are relevant resources in today's societies [8, 11, 12]. Copper is the third most important metal by weight [13]; its yearly production is estimated at 16 million tons [9, 14] and is used in electrical equipment (60% of its consumption), plumbing/construction, machinery, transport, coins, art, music instruments, kitchen utensils [11, 13], and to catalyze many reactions [15–17]. Copper is also a micronutrient in animals and plants. Lead and its related compounds are very toxic [18]. Most recent uses of lead [18] have been banned, such as gasoline additives, in solders, paint pigments, and the EU plans to ban lead ammunition and fishing gear [19]. It is still used for lead-acid batteries and as radiation shields [11]. No biological functions are known [18]. Cadmium is highly toxic. It can be applied as a stabilizer in plastics, pigment in dyes, coating agents, accessories/jewelry, Ni-Cd rechargeable

batteries, and solar cells [20, 21], with the latter two contributing to impulse its use [21]. The EU has banned it from being used in plastics, paints, and jewelry [22]. In this paper, we focus our particular interest in nickel due to its increasing market value. Nickel is ferromagnetic at room temperature [11] and is known to catalyze reactions [23]. It is used for the production of metal alloys (stainless steel totals 75% of its consumption [24]), nickel cast iron (jewelry, coins), corrosion-resistant coatings by electroplating, and the production of batteries (nickel-metal hydride and Li-ion) [11, 25, 26]. Nickel has biological functions in plants and cyanobacteria [26]. Due to the aforementioned reasons, nickel is a valuable metal, so the minimization of its pollutant discharges, through separation and recovery, has economic impact on businesses. Furthermore, these also contribute to a more circular and sustainable economy, which many countries are promoting.

Several treatment techniques can be applied to remove heavy metals from wastewaters. These were fully described in a recent review of the authors [1]. However, only a few can be used for the simultaneous goal of recovering the cation being removed from water: ion exchange [27–29], adsorption [30–36], and electroplating [27, 28, 37] are the most effective ones. As such, operating these methods with high efficiency and low-cost at large scale is crucial to promote the recovery of metals as valuable resources. Both adsorption processes rely on the development of high performing materials (the ion exchanger and adsorbent, respectively) that are modified to be selective, while electrolysis can be employed for multiple species by assembling an electrolytic cell and adjusting electric potential on demand. However, a major drawback relies on the fact that electrochemical processes are expensive and only viable in cases where wastewater are not highly contaminated. On the other hand, adsorption processes are simple in operation and design, and their cost is mostly associated with the sorbent materials [27, 28, 37]. Natural materials as well as engineered ones have been used as adsorbents for heavy metals, and the number of published research on the topic has been increasing [1].

Schiff bases are the most common family of molecules used as nickel ionophores [38]. They are considered a subclass of imines and are obtained by a condensation reaction of a primary amine and a carbonyl precursor, e.g., an aldehyde [39]. These molecules can be multidentate and are generally based on nitrogen or oxygen donors but can also include phosphor and sulfur [39]. The formation of the ligand-nickel (II) complex was studied with different Schiff bases by several authors developing colorimetric nickel sensors (in which the response to the cation is measured by absorbance in the ultraviolet-visible region or by fluorescence), and it was found that the stability constant is very high ($\log K > 5$) [40–44]. Ganjali et al. [43] confirmed the ligand's selectivity by evaluating the stability constant towards copper ($\log K = 5.9$ for Ni (II) vs. 4.2 for Cu (II)).

A particular case of Schiff base, salens (symmetrical tetradentate molecules with two nitrogen and two oxygen donor atoms [39]) were studied by Gupta and coauthors [44, 45]. They have successfully used salens as ionophores in ion sensing electrodes with poly(vinyl chloride) membranes [44, 45]. In one of the works, the authors have proposed two distinct molecules as nickel ionophores (Figure 1), both with very high affinity for nickel ($\log K > 7$ for Ni (II) and <4.2 for the remaining cations) [44]. In the literature, the use of salens can also be found for the modification of MCM (Mobil Composition of Matter) and SBA (Santa Barbara Amorphous) particles [46–52], silica gel [53], or silica composites [54], in order to promote salen-metal cation complexes. However, only three works using silica-based materials, by Enache et al. [52], Kursunlu et al. [53], and Qiao et al. [54], are reporting adsorption studies. It should be mentioned that salens are also reported as copper ionophores [55, 56], responding selectively to this cation and exhibiting very high stability constants ($\log K = 4.2$ [55] or 8.4 [56]). So, the selectivity of the Schiff base ligand must be influenced by the nonelectron donor groups in the molecule that affect, for instance, its overall size and accessibility of ions to the electron donor groups.

In this work, we report the development of a selective adsorbent for nickel, obtained by modifying the silica matrix of a silica aerogel with hemi-salen functional groups. Thus, a highly porous and selective adsorbent is obtained. To the best of our knowledge, it is the first time a silica aerogel is modified using such a functional group. The modified aerogel-like monolith is tested in batch tests to assess its suitability and selectivity against common relevant cations.

2. Materials and Methods

2.1. Materials. As silica sources, methyltriethoxysilane (MTES, ≥99%), tetraethyl orthosilicate (TEOS, 98%), and (3-aminopropyl) trimethoxysilane (APTMS, ≥97%) were purchased from Sigma-Aldrich and used as received. Salicylaldehyde (*p.a.*, Merck) was used to obtain the hemi-salen modifying groups on the silica matrix. Anhydrous oxalic acid (≥99%, Sigma-Aldrich) and ammonium hydroxide (25% NH_3 in H_2O, Sigma-Aldrich) were the sol-gel chemistry catalysts. Methanol (MeOH, 99.8%, VWR) and ethanol (EtOH, ≥99.8%, Fisher) were used as solvents. Deuterated methanol (CD_3OD, 99.8%, Eurisotop) and 3-(trimethylsilyl) propionic acid sodium salt (TMSP, 98%, Eurisotop) were used as solvent and internal reference for NMR spectroscopy. Heavy metal solutions were prepared using copper (II) nitrate hemipentahydrate (*p.a.*, Chem-Lab), lead (II) nitrate (≥99.0%, Sigma-Aldrich), cadmium (II) nitrate tetrahydrate (≥99.0%, Sigma-Aldrich), and nickel (II) nitrate hexahydrate (crystals, Sigma-Aldrich). High purity water was used whenever needed. Nitric acid (65%, Fisher) was used to adjust the pH of solutions.

2.2. Modification of APTMS Co-precursor. The addition of a Schiff base functional group to the silica matrix was achieved by modifying the organic group in a silicon alkoxide precursor. The reaction between the primary amine of APTMS and salicylaldehyde was promoted [46, 47], resulting in a hemi-salen modified silica precursor (HSPTMS, (E)-2-(((3-(trimethoxysilyl)propyl)imino)methyl)phenol), as shown in Figure 2.

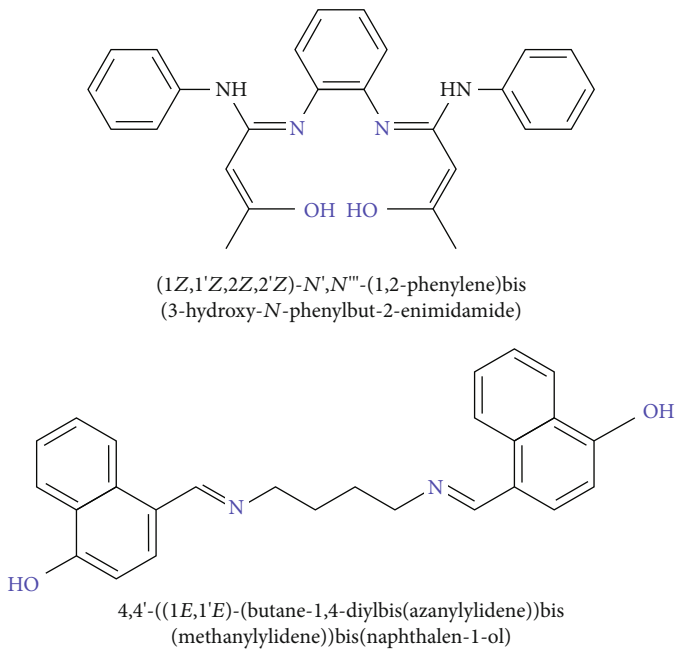

Figure 1: Representation of the ionophore molecules developed by Gupta et al. [44]. Proposed groups responsible for cation sorption are presented in blue.

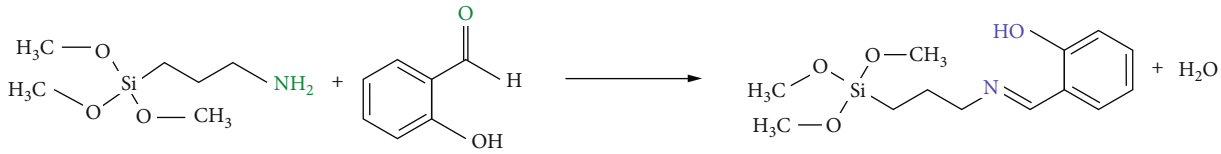

Figure 2: Schematic representation of the HSPTMS formation reaction. Proposed groups responsible for cation adsorption are presented in blue, and the groups that take part in the reaction are shown in green.

APTMS and salicylaldehyde were mixed in methanol with a 10 mol% excess of salicylaldehyde. This mixture, labelled as A, was stirred until homogenization and left to react in an oven for 24 hours at 27°C. The mixture turned yellow instantly, indicating the formation of the hemi-salen.

2.3. Synthesis of Schiff Base-Modified ORMOSIL Aerogel-Like Monolith. To prepare silica aerogels with the HSPTMS precursor, MTES was diluted in methanol and hydrolyzed (0.1 M oxalic acid). After one day, the hydrolyzed MTES, mixture B, was mixed with the so-called mixture A and stirred. After a couple of minutes, TEOS and then the basic catalyst (1 M ammonium hydroxide) were added. All sol-gel steps were carried out at 27°C. The Si: solvent: water molar ratios in the sol were kept at 1 : 12 : 8, and the silica co-precursors were mixed in an 50/35/15 molar percentage for MTES, TEOS, and HSPTMS, respectively. Gelation and aging occurred in an oven at 27°C for six days. Aged gels were demolded and washed by being immersed in hot ethanol for a total of six days, with ethanol being changed every day. Finally, the gel monoliths were dried in an oven for three days at 60°C.

2.4. Characterization. The formation of HSPTMS was investigated via NMR (Bruker Biospin GmbH, ^{1}H spectra collected at 400 MHz and ^{13}C spectra collected at 100 MHz). ^{1}H and ^{13}C spectra for both reactants and HSPTMS were obtained by dissolution in deuterated methanol. The analysis of the ^{13}C spectrum did not contribute with additional information relatively to the ^{1}H spectrum analysis, and thus, it is not shown. HSPTMS was obtained directly from mixture A via evaporation of the solvent.

The characterization routines of aerogels are described in previous works by the authors [57, 58]. Bulk and skeletal densities were used to obtain adsorbent porosity. Bulk density of the adsorbents was obtained by weighting the samples and measuring their dimensions on the three axes. Skeletal density was obtained with ground samples by He pycnometry (Accupyc 1330, Micrometrics). Linear shrinkage was calculated from the change in diameter of the dried sample comparatively to the gelation mold. The BET specific surface area was obtained through nitrogen adsorption (ASAP 2000, Micrometrics). Pore volume and average pore size were calculated in accordance with a previous work [59]. Microstructure observation was performed with field-emission scanning electron microscopy (FE-SEM) (Merlin Compact/VPCompact FESEM, Carl Zeiss Microscopy GmbH) [60, 61]. Fourier transform infrared spectroscopy (FTIR) (FT/IR 4200, Jasco) was performed, being the spectra obtained with KBr pellets in the wavenumber range of 4000 to 400 cm^{-1}, with 128 scans and a resolution of 4 cm^{-1}. C, H,

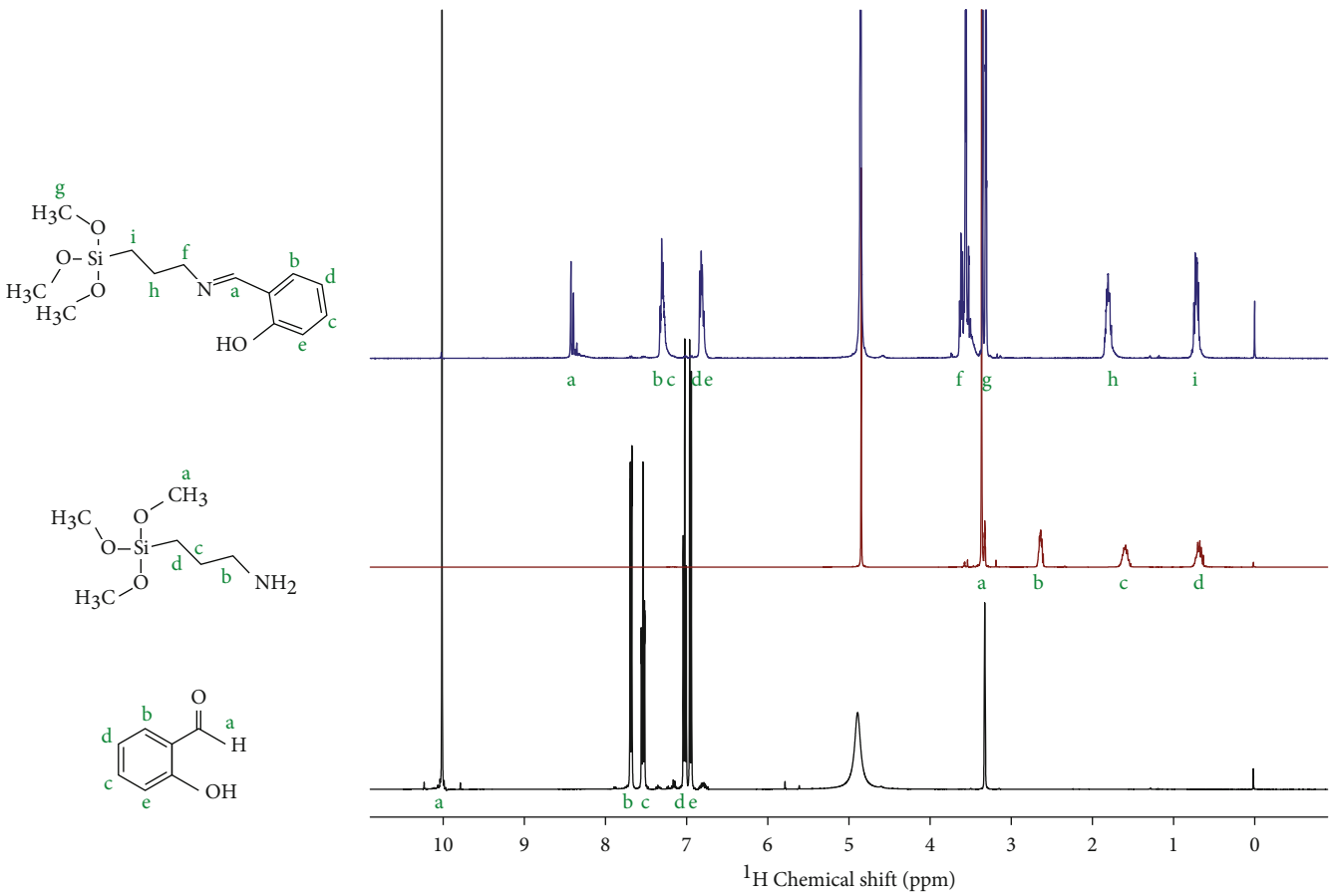

Figure 3: ^{1}H NMR spectra for salicylaldehyde, APTMS, and HSPTMS.

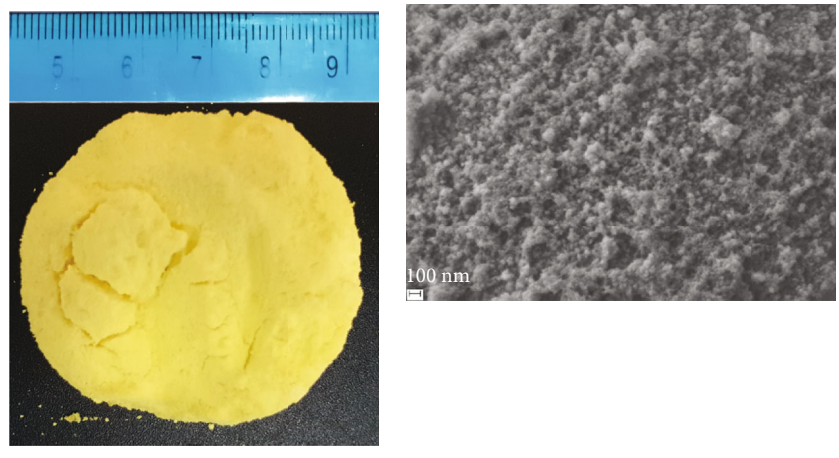

(a) (b)

Figure 4: Photograph (a) and micrograph at ×30 k magnification (b) of the Schiff base-modified aerogel.

Table 1: Physical/structural properties of the functional aerogel-like monolith adsorbent.

Bulk density (g cm^{-3})	Skeletal density (g cm^{-3})	Porosity (%)	Linear shrinkage (%)	S_{BET} (m^2 g^{-1})	V_{pore} (cm^3 g^{-1})	D_{pore} (nm)
0.22 ± 0.04	1.396 ± 0.004	85 ± 3	10 ± 3	27.7 ± 0.3	3.9 ± 0.8	563 ± 122

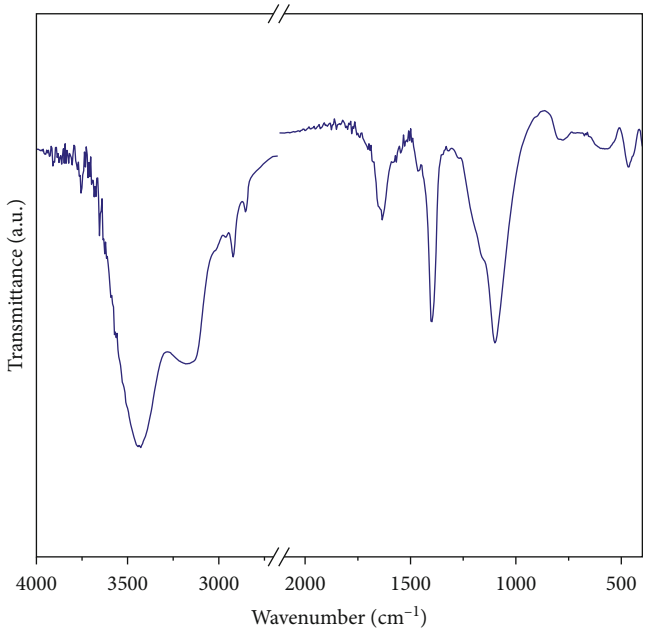

Figure 5: Infrared spectrum of the adsorbent.

Table 2: C, H, and N contents of the Schiff base-modified aerogel-like monolith.

Sample/hypothesis	wt% C	wt% H	wt% N
Complete condensation	27.0	3.7	2.4
Incomplete condensation 1OH	25.1	4.5	2.2
Incomplete condensation 2OH	22.9	5.1	2.0
Experimental values	24.4 ± 2.0	3.6 ± 0.1	2.5 ± 0.1

and N content of powdered samples was determined by elemental analysis (EA 1108 CHNS-O, Fisons). Zeta potential measurements of an aqueous suspension of the sample nanoparticles (0.1%, *w*/*v*) at pH 4 were carried out by electrophoretic light scattering (Zetasizer NanoZS ZN 3500, Malvern Instruments); the suspension was dispersed in an ultrasound bath for 10 minutes, and the pH was adjusted by the addition of HCl just before measurements. The elemental composition of loaded adsorbent samples was estimated with energy-dispersive X-ray spectroscopy, EDS (X-Max^N Silicon Drift EDS Detector, Oxford Instruments).

Heavy metal concentration in solutions was determined by flame atomic absorption spectroscopy (AAS) with an acetylene-air flame (939 AAS, Unicam).

To provide insight on the interactions with the different ions, the geometry of hydrolyzed HSPTMS in water was computed. The system was composed of a box, with the precursor molecule surrounded by 632 water molecules, of dimensions 2.6520 nm × 3.1410 nm × 2.4120 nm, and with full periodic boundary conditions. The simulation was conducted in CP2K v7.1 [62] using the Geometry, Frequency, Noncovalent, eXtended Tight Binding (GFN-xTB) with the DFT-D3 dispersion correction [63, 64] as electronic model.

2.5. Adsorption Tests. Adsorption experiments followed the procedures used previously [57, 58, 65]. The aerogel-like monolith was prepared for adsorption by milling and selecting particles within a size range of 75 to 250 μm. Batch adsorption tests were conducted by mixing the powdered adsorbent and the cation solution in a test flask, shaken in a rotational stirrer at speed setting 16 rpm (REAX 20, Heidolph Instruments) with an adsorbent dose of 2 g L^{-1} at pH 4 and 25°C. When the test ended, the solution was filtered, and the concentration of the filtrate was determined. For comparison, a silica aerogel without the Schiff base modification was tested in the same conditions.

Isotherm studies were performed by varying the adsorbate concentration from 20 to 500 mg L^{-1} and conducted for 24 h. The selectivity of the Schiff base ORMOSIL aerogel-like monolith was studied in batch kinetic tests, with contact times ranging from 5 minutes to 24 h, with an adsorbate concentration of 100 mg L^{-1} per cation. Binary mixtures containing copper and mixtures containing nickel plus copper and nickel ions isolated were tested.

The viability of recovering the adsorbed nickel was assessed by a desorption test performed with HCl and HNO_3 on nickel loaded particles (from the isotherm studies with a starting concentration of 100 mg L^{-1}). The loaded adsorbent was shaken with a 1 M solution of the desorption agent for three hours.

A minimum of two replicates were obtained for all reported data points.

2.6. Analysis of Adsorption Data. All physical quantities and adsorption model parameters here described are defined with mass units. While discussing binary mixtures, these are expressed in molar units when required. Adsorption capacity (q_t or q_e if equilibrium is reached, mg g^{-1}) was calculated from the initial (C_0, mg L^{-1}) and final concentrations (C_t or C_e, mg·L^{-1}, respectively), adsorbent mass (m, g), and solution volume (V, L) according to Equation (1). Time t is expressed in hours. Selectivity was calculated with Equation (2) using the molar adsorption capacity after 24 hours.

$$q = \frac{V(C_0 - C)}{m}, \tag{1}$$

$$\alpha_{1,2} = \frac{q_1}{q_2}. \tag{2}$$

Freundlich, BET, and Langmuir-Henry models were fitted to the equilibrium data to interpret the metal ion-adsorbent interactions. The pseudo-first order and pseudo-second order models, as well as a modified pseudo-second order model that considers an initial adsorption, were tested to describe the kinetic data. The fits were performed using nonlinear algorithms, and their quality was assessed using Akaike and Bayesian information criteria [66].

The Freundlich model [67], Equation (3), describes the adsorption on heterogeneous surfaces [68]. It has two parameters: the Freundlich constant, K_F ((mg g^{-1})(L mg^{-1})$^{1/n_F}$), that gives the relative adsorption capacity of the adsorbent, and the heterogeneity factor $1/n_F$. The BET model [69] describes multilayer adsorption and was

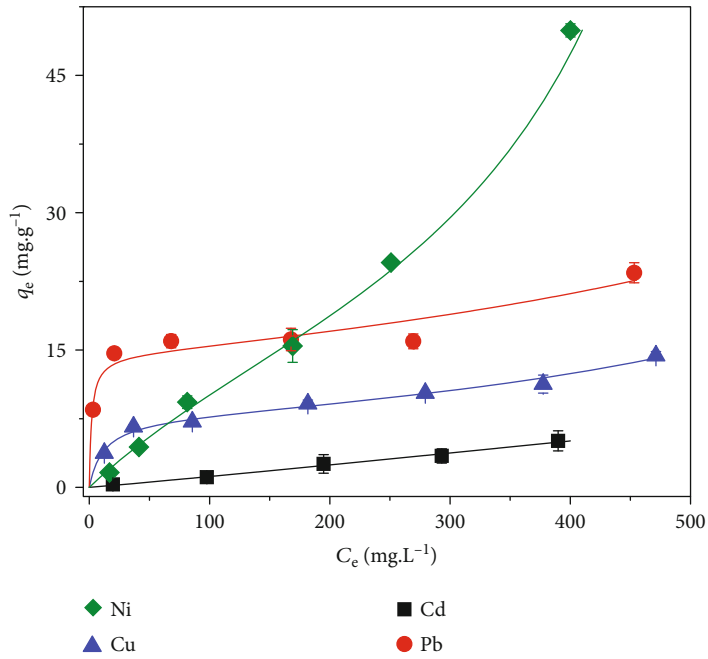

Figure 6: Adsorption isotherms in single-metal solutions.

Table 3: Fit parameters for the isotherm models and maximum uptake by Schiff base-modified aerogel-like monolith.

	Ni	Cd	Cu	Pb
$q_{e,max}$ exp (mg g^{-1})	49.9	5.1	14.4	23.4
		BET model		
q_m (mg g^{-1})	19 ± 2	4 ± 2	7.6 ± 0.4	14 ± 1
$K_L \times 10\text{^}3$ (L mg^{-1})	7 ± 2	4 ± 3	87 ± 24	524 ± 268
$K_S \times 10\text{^}3$ (L mg^{-1})	1.6 ± 0.0	1.2 ± 0.3	0.99 ± 0.08	0.8 ± 0.2
AIC	18	22	5	30
BIC	−3	−19	−8	10
		Freundlich model		
$1/n_F$	1.3 ± 0.1	1.1 ± 0.1	0.33 ± 0.04	0.16 ± 0.04
K_L (L mg^{-1})	$(2 \pm 1) \times 10^{-2}$	$(9 \pm 4) \times 10^{-3}$	1.7 ± 0.4	8 ± 2
AIC	21	−6	7	230
BIC	13	−18	1	15
		Langmuir-Henry model		
q_m (mg g^{-1})	[a]	[a]	6.6 ± 0.9	14 ± 2
K_F (mg g^{-1} (L mg^{-1})$^{1/n_F}$)	[a]	[a]	0.12 ± 0.07	0.5 ± 0.3
$K_H \times 10\text{^}3$ (L g^{-1})	[a]	[a]	15 ± 3	17 ± 6
AIC	[a]	[a]	11	32
BIC	[a]	[a]	−2	12

[a]The model did not fit to the data.

conceptualized for the adsorption of gaseous species. It can be expressed for liquids with Equation (4) [70], in which q_m represents the monolayer adsorption capacity (mg g^{-1}), K_L is the equilibrium constant for the first adsorbate layer (L mg^{-1}), and K_S is the equilibrium constant for the upper layers. C_{BET} is equal to K_L divided by K_S. The Langmuir-Henry model, Equation (5), combines both the Langmuir and Henry isotherms [71], describing adsorption both at active surface sites and by the dissolution of the sorbate inside the porous matrix. K_L is the Langmuir constant and has the same meaning as in the BET isotherm (L mg^{-1}), and K_H is the Henry constant (L g^{-1}).

$$q_e = K_F C_e^{1/n_F}, \quad (3)$$

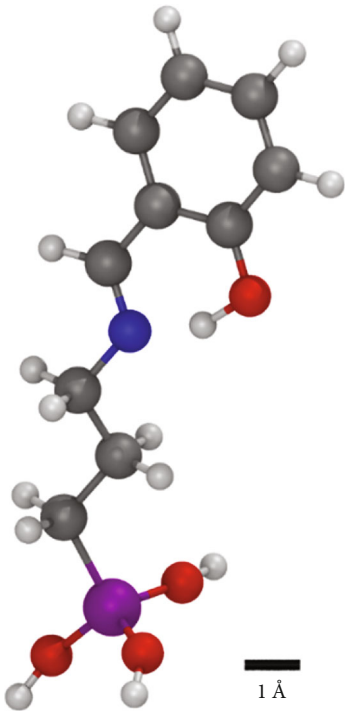

Figure 7: Representation of the optimized structure of the hydrolyzed HSPTMS coprecursor.

$$q_e = \frac{q_m K_L C_e}{(1 - K_S C_e)(1 - K_S C_e + K_L C_e)}, \quad (4)$$

$$q_e = \frac{q_m K_L C_e}{1 + K_L C_e} + K_H C_e. \quad (5)$$

In the kinetic models used, the equilibrium uptake or adsorption capacity, q_e, is a model parameter. In the pseudo-first order model [72], Equation (6), k_1 is the first order rate constant (h^{-1}). This model reveals that the adsorption is controlled by diffusion. A modified pseudo-second order equation, considering an initial adsorption, reveals an adsorption process controlled by the surface reaction and is described in Equation (7). In this model, q_0 ($mg\,g^{-1}$) represents the initial uptake, and the pseudo-second order adsorption rate constant corresponds to k_2 ($g\,mg^{-1}\,h^{-1}$). If the initial uptake is negligible, the equation is reduced to the pseudo-second order model [73]. It was verified that modified silica-based aerogels adsorb heavy metals very quickly [58]; hence, an initial uptake of sorbate can be considered in some cases. This can be attributed to the metal amount adsorbed during the preparation of the tests (which is sometimes observed by changes in the aerogel color), before the flasks are shaken, which is considered the effective start of the test. The modified pseudo-second order model can describe these situations.

$$q_t = q_e\left(1 - e^{-k_1 t}\right), \quad (6)$$

$$q_t = q_0 + \frac{q_e^2 k_2 t}{q_e k_2 t + 1}, \quad (7)$$

The intraparticle diffusion and Boyd models were further applied to have a deeper analysis of the adsorption of nickel on the aerogels (a similar analysis was not possible for copper due to its fast adsorption). The intraparticle diffusion model (presented by Weber and Morris) is based on Fick's 2nd law equation [74, 75] and can be described through Equation (8)

$$\frac{q_t}{q_e} = A_{0,i} + k_{P,i} t^{0.5}, \quad (8)$$

where A_0 is a constant related with the thickness of the boundary layer, k_P ($s^{-0.5}$) is the rate constant and depends on the diffusion coefficient, and i is related with the number of steps governing the adsorption process. On the other hand, the Boyd model (also based on Fick's 2nd law equation) was also shown to predict the rate limiting step through the computation of the intercept of a linear equation described as $B_t = mt + y_0$, where B_t is defined by Equation (9) for short adsorption times.

$$B_t = 2\pi - \frac{F\pi^2}{3} - \left(1 - \frac{\pi F}{3}\right)^{1/2} \quad (0 < F < 0.85), \quad (9)$$

$$F = \frac{q_t}{q_e}. \quad (10)$$

If $y_0 = 0$, the rate limiting step is intraparticle diffusion; otherwise, film diffusion model governs the process [76, 77].

3. Results and Discussion

3.1. Schiff Base Reaction. The formation of HSPTMS, via the reaction illustrated in Figure 2, was studied, and the NMR spectra are presented in Figure 3. The formation of HSPTMS can be observed, namely, by the disappearance of the carbonyl group from salicylaldehyde (peak a, δ ~10 ppm) and the amine group in APTMS (peak b, δ ~2.7 ppm) in the product, and the appearance of a new proton associated with the C=N bond (peak a, δ ~8.4 ppm). Protons associated with the methoxy groups and propyl chain did not suffer changes in their chemical environment, while the ones associated with the aromatic ring (peaks b-e in the salicylaldehyde and HSPTMS spectra) suffered some alterations, due to a new chemical environment.

3.2. Modified Aerogel-Like Monolith Characterization. The obtained modified silica aerogel-like monolith and its porous morphology are depicted in Figure 4. The physical/structural properties of the adsorbent are summarized in Table 1.

The ORMOSIL aerogel-like monolith samples feature a distinctive bright yellow color, due to the presence of the hemi-salen. Despite being dried by evaporation of the solvent, the gel remained a monolith and exhibits a small radial shrinkage, resulting in a bulk density and porosity similar to that of amine modified silica aerogels and contrasting to their xerogel counterparts [58]. The skeletal density of this adsorbent is lower than that of silica, as it is observed with

Table 4: Fitting parameters of the kinetic models for the total adsorption in binary mixtures.

	Modified pseudo-second order model					Pseudo-first order model			
	$q_0 \times 10^2$ (mmol g^{-1})	$q_e \times 10$ (mmol g^{-1})	k_2 (g mmol^{-1} h^{-1})	AIC	BIC	$q_e \times 10$ (mmol g^{-1})	k_1 (h^{-1})	AIC	BIC
Ni + Cd	9 ± 1	2.3 ± 0.2	0.8 ± 0.3	−10	−51	2.5 ± 0.3	0.9 ± 0.4	−32	−40
Ni + Cu	[a]	3.7 ± 0.3	142 ± 68	−59	−63	3.6 ± 0.1	23 ± 7	−55	−59
Ni + Pb	7 ± 2	2.8 ± 0.3	0.4 ± 0.2	−9	−50	2.6 ± 0.2	0.3 ± 0.1	−38	−46
Cu + Cd	[a]	1.7 ± 0.4	32 ± 29	−27	−39	1.6 ± 0.2	8 ± 6	−24	−37
Cu + Pb	[a]	1.3 ± 0.2	51 ± 32	−47	−55	1.3 ± 0.1	4 ± 1	−46	−54

[a]Negligible value.

ORMOSIL aerogels. As expected, the modification of the silica matrix with the Lewis base group impacted the structural properties of the adsorbent, as this sample is less porous (and hence, denser) than other ORMOSIL aerogels (without Lewis base groups) or native silica aerogels [58, 59, 78, 79]. For the Schiff base-modified aerogel-like monolith, hydrogen bonding with solvent molecules does not counter the effect of nonhydrolysable apolar groups in the network, resulting in low capillary stresses during solvent evaporation and low shrinkages in the final material. This result can be due to: the presence of the azomethine group (imine) instead of a primary or secondary amine in amine modified gels; and/or the high pore radius. Thiol modified silica xerogels also retained monolithity after evaporative drying, and their properties are similar to the aerogel counterparts [57, 80]. The specific surface area of this adsorbent is small, even when compared to other ORMOSIL aerogels, and is due to the predominant macroporous nature of the material, as indicated by the average pore size in Table 1. Previous works show that, in some situations, the specific surface area does not make a significant impact in adsorption performance [58, 80].

The FE-SEM image depicted in Figure 4(b) confirms the high porosity of the sample, revealing numerous voids with a wide distribution of pore sizes. In fact, many pores smaller than the average pore size estimated (563 nm, Table 1) are observable in this image. The pearl necklace type of microstructure expected from silica aerogels is visible. Additionally, the secondary silica particles are very small and seem to be poorly individualized, surely due to the extended aging period. This microstructure is similar to that of amine modified aerogels recently reported by the authors [58]. The evaluated structural properties allow to conclude that the prepared sample can be considered an aerogel, according to the different proposals for this definition [79, 81–83].

The FTIR spectra and the C, H, and N compositions of the aerogel-like monolith are presented in Figure 5 and Table 2, respectively. The interpretation of the experimental results obtained by elemental analysis relies on theoretical assumptions regarding the condensation of hydrolyzed precursor molecules in the sol, previously detailed by the authors [65].

The FTIR spectrum of the adsorbent reveals the formation of the silica matrix and the incorporation of the Schiff base in its structure. Bands associated with siloxane bonds are visible at 577, 1099, and 1162sh cm^{-1}; bands associated with the ortho substituted benzene ring are visible at 1464 and 3100 cm^{-1}, and the bonded hydroxyl groups generate a broad band at 3431 cm^{-1}. Some bands are resultant from the overlap of different functional groups that vibrate at similar frequencies. The bands at 465 and 791 cm^{-1} are the result of overlapping vibrations from siloxane bonds and the benzene ring, while the band at ~1632 cm^{-1} results from the overlapping of multiple bond stretching of the benzene group, the azomethine bond, and the hydroxyl groups. These bonds limit the conclusions gained from this analysis. The remaining bands are due to the methyl and methylene groups in the MTMS and HSPTMS precursors.

Analyzing the carbon content of the sample, the elemental analysis reveals that hydrolysis is not complete, suggesting an incomplete condensation of one hydroxyl group per Si. This result can be justified by the fact that HSPTMS co-precursor may undergo incomplete hydrolysis, in comparison to the remaining co-precursors, due to its slower reactivity and to it being added just before the base. Furthermore, the large organic group in this co-precursor is likely to hinder the formation of siloxane bridges. The nitrogen content in the sample is superior to the predicted, which can be related with the presence of ammonia residues even after the washing stage, as found before in samples without nitrogen-containing precursors [58]. The experimental value obtained indicates that there are 1.8 mmol of hemi-salen groups per gram of adsorbent or 3.9×10^{19} active sites per square meter. It was verified experimentally by EDS that the distribution of the coprecursors in the aerogel-like monolith matrix is not homogenous, as expected. Nitrogen was not detected with statistical significance in some portions of sample, and in others reached 4 wt%. The hydrogen content is inferior to the predicted, but this element is also more affected by the randomness of the network ramification. The excess of salicylaldehyde seems to be completely removed by the washing stage, as the carbon content would exceed the predictions if otherwise.

The addiction of the hemi-salen groups caused the silica surface to feature a positive charge (24 ± 1 mV), at the conditions for cation adsorption, instead of a negative charge found in nonmodified silica aerogels. Positive zeta potentials were also reported for amine-modified silicas [84–86]. In fact, it is known that inner-sphere complexation, mechanism in which the cation is adsorbed by losing its hydration shell and forming chemical bonds with the adsorbent, is insensitive to the surface charge of the adsorbent [87]. By contrast,

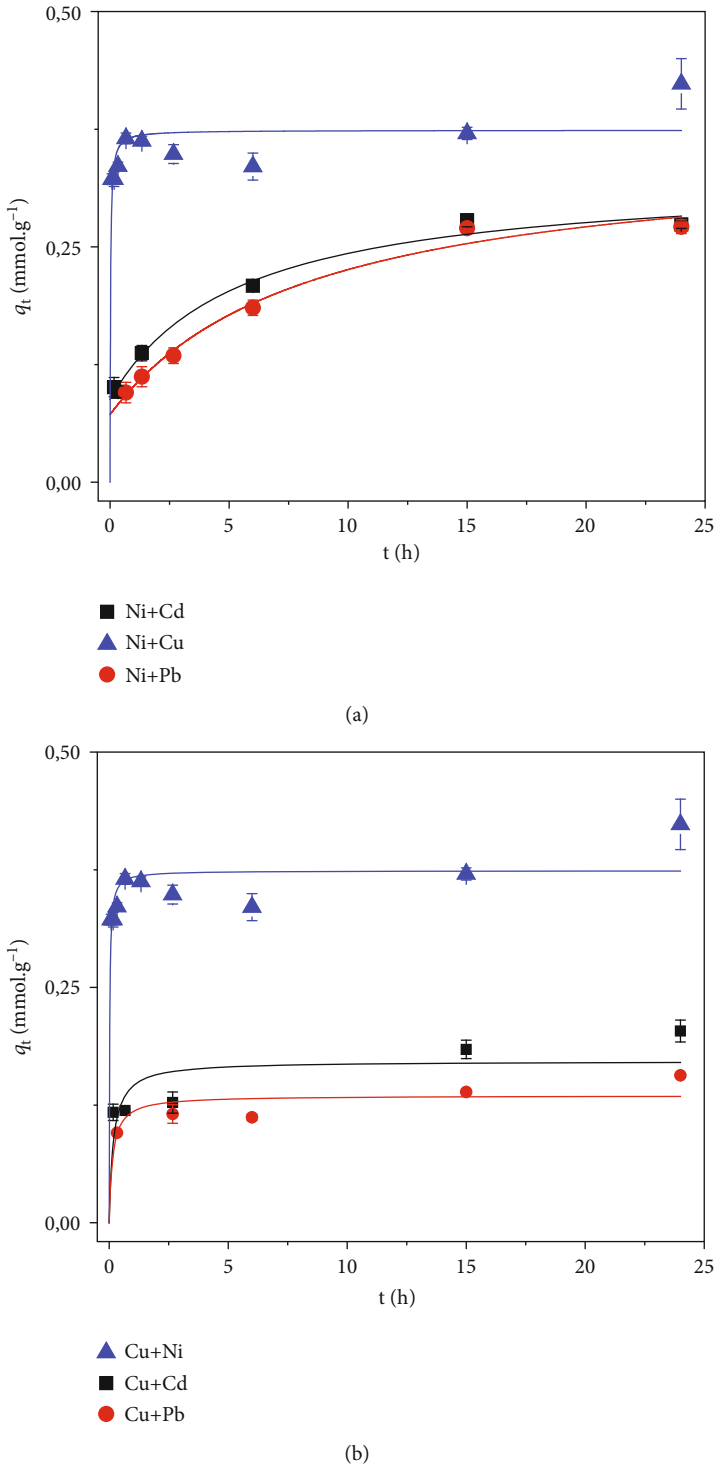

Figure 8: Adsorption kinetics for the total uptake in binary mixtures of (a) nickel and (b) copper.

if the adsorption of cations is due to electrostatic forces or hydrogen bonding, it is only verified on a negatively charged adsorbent surface [87].

3.3. Adsorption Isotherms and Mechanisms. The experimental data and the best isotherm fit are presented in Figure 6. The fit parameters for the studied models are reported in Table 3.

Nickel removal, cation for which some salens were shown to be ionophores, was the highest observed out of the four cations studied. This was expected, given the high formation constants of nickel-Schiff base complexes. From the statistically point of view, the BET model represented the data the best for the adsorption of nickel, copper, and lead, as the data points seem to follow a type II isotherm (gas isotherm classification) [88] or an L3 isotherm (solid-

Table 5: Fitting parameters of the kinetic models for the adsorption of nickel and copper isolated and in the presence of interfering ions.

	Modified pseudo-second order model					Pseudo-first order model			
	q_0 (mg g^{-1})	q_e (mg g^{-1})	k_2 (g mg^{-1} h^{-1})	AIC	BIC	q_e (mg g^{-1})	k_1 (h^{-1})	AIC	BIC
Ni	4.7 ± 0.8	17 ± 3	$(5 \pm 3) \times 10^{-3}$	24	4	16 ± 2	0.3 ± 0.1	25	19
Ni (w/Cd)	3.7 ± 0.6	15 ± 2	$(8 \pm 3) \times 10^{-3}$	18	−2	14 ± 1	0.3 ± 0.1	20	14
Ni (w/Cu)	[a]	15 ± 2	$(5 \pm 3) \times 10^{-2}$	21	8	13 ± 1	0.5 ± 0.2	24	12
Ni (w/Pb)	[a]	14 ± 1	$(2.3 \pm 0.7) \times 10^{-2}$	9	1	13 ± 1	0.3 ± 0.1	14	6
Cu	[a]	5.5 ± 0.4	1.0 ± 0.3	2	−11	5.4 ± 0.2	2.8 ± 0.6	5	−8
Cu (w/Ni)	[b]	[b]	[b]	[b]	[b]	[b]	[b]	[b]	[b]
Cu (w/Cd)	[a]	10 ± 1	0.13 ± 0.07	17	5	9 ± 1	0.8 ± 0.3	21	9
Cu (w/Pb)	[a]	8.0 ± 0.8	0.7 ± 0.3	5	−4	7.5 ± 0.4	4 ± 1	10	1

[a]Negligible value. [b]System is always at equilibrium—Figure 8(b).

liquid isotherm classification) [89], which is less defined in nickel adsorption. Thus, the adsorption by the Schiff base-modified ORMOSIL aerogel-like monolith is suggested to occur in multilayers of adsorbate deposited on the surface of the adsorbent. However, understanding how metal ions can form multilayers by adsorption onto an ionophore-containing surface is not straightforward. In fact, the adsorption of metal ions from aqueous media is generally controlled by adsorbent surface chemistry and surface area [90] and occurs in the form of coordination bonds [91–98]. In fact, in other materials modified with Lewis bases, the multiple neighboring functional groups participate in the complexation of one cation, and the complexing amine groups can even replace water molecules from the primary hydration shell (which is known as inner-sphere complexation) [91, 95, 96, 99, 100]. The interaction of Lewis base-modified adsorbents with the heavy metal cations may be explained by the Pearson acid-base concept. Thus, the results reported in this work follow a different trend compared to amine modified silica aerogels [58] or similar materials for which the Langmuir model fitted to the data the best in most situations [52–54]. However, by the way the data is presented in the literature, we cannot conclude if testing higher cation concentrations would produce an isotherm shaped like a BET curve. Even so, it should be highlighted that a multilayer-like adsorption for metal ions has been previously reported [101–104]. Furthermore, in a previous work, the existence of multiple types of surface groups available for adsorption generated a L4 isotherm for copper [58]. Different hypotheses for this observation can be raised and are discussed as follows.

The adsorption isotherms can be due to a combination of different factors: the macroporous nature of the adsorbent [88] and the affinity between adsorbate layers, as relevant as cation-adsorbent interactions [89], assuming that multilayers are present. The latter means that adsorption is not an exclusive result of the interaction with active surface sites. Multilayer adsorption is commonplace in the adsorption of organic pollutants due to van der Waals or π-π interactions; however, cations would repel each other. Some anions may interact with the adsorbed cation layer [105]; based on that, Jorgetto et al. [106] proposed that the BET isotherm reflects multiple adsorbate layers due to the electrostatic interactions between alternating layers of cations and counter-ions in solution. However, this situation does not seem so likely with the nitrate anions used in this work [105]. To evaluate the possibility of multilayer of adsorbed cations at the surface of the adsorbent, energy dispersive X-ray analysis (EDS) was conducted with the loaded adsorbent particles. The presence of cations at the surface was not detected (data not shown), with one exception for copper. In a previous work, SEM and EDS analyses showed that the loaded adsorbent particles were coated by metal salts, possibly due to nucleation induced by adsorbed species or to chemical precipitation at the surface of the adsorbent [80]. Such behavior was not observed in this work, and the microstructure of the loaded adsorbent simply seemed more closed (data not shown). This was expected as the loaded particles were dried by evaporating water, which increases capillary pressure in the pores by forming hydrogen bonds with the solid. Only when analyzing a large sample area could the presence of some copper (as high as 2.5 ± 0.2 wt%) be detected. The implication of this observation is further discussed later.

To obtain further insight on this matter, the hybrid Langmuir-Henry model (Equation (5)) was analyzed (Table 3). This considers the possibility of the structure of water molecules inside the adsorbent's pores to be different than in the liquid water (bulk) allowing the dissolution of different amount of electrolyte, in addition to adsorption at active surface sites. If that is occurring, the hybrid Langmuir-Henry model would fit better to experimental data, which is not the case. Lead is the only cation for which the plateau corresponding to the monolayer adsorption capacity is well-defined, resembling a Langmuir curve, suggesting that the cation-adsorbent interactions are strong in this case, and AIC and BIC do not agree on the preferred model; however, we can observe that the data resembles the BET curve.

Based on the previous observations, we must conclude that in spite of the BET model represented the data the best for nickel, copper, and lead, the adsorption of these cations does not occur in multilayers. As such, the increase in adsorption capacity after a plateau (saturation of active sites) may simply reflect changes in the adsorbent's surface/active

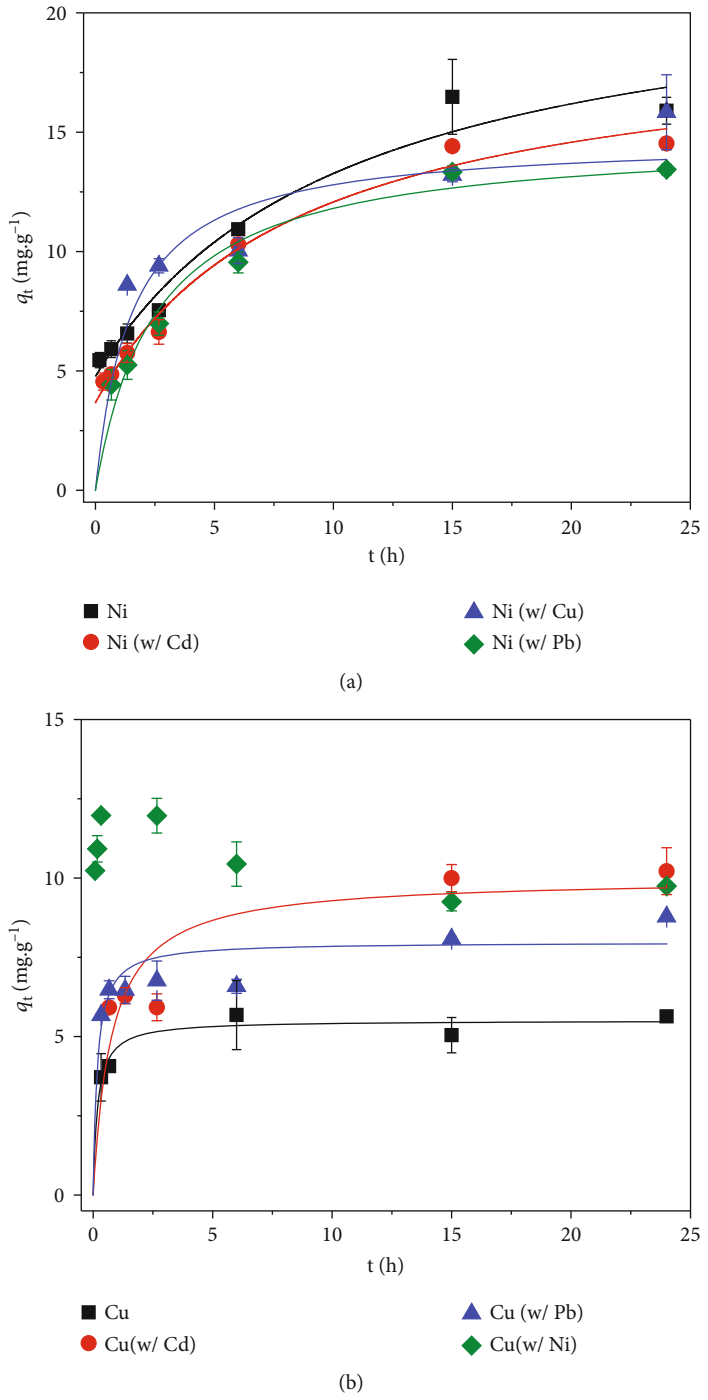

Figure 9: Adsorption kinetics for (a) nickel and (b) copper, isolated and in binary mixtures.

site availability (e.g., by rearranging of adsorbed species) or the occurrence of metal nucleation induced by the salen-metal initial interaction [107–109]. EDS spectra support this conclusion, since some copper was quantified using a large area of sample.

A different but related question that shall be addressed is the interaction mechanism between metal ions and the Schiff base. At the highest equilibrium concentration, the Schiff base: Ni ratio is 2 : 1. It could be said that not all potential adsorption sites are occupied; however, as mentioned before, it was proposed that neighboring Lewis base groups are involved in the complexation of one cation. Hence, it is possible that all Schiff base groups in the aerogel are involved in the adsorption process. This hypothesis is explored again below. Nonspecific interactions, like electrostatic interactions, cannot occur with the positively charged surface of the modified silica aerogel-like monolith. The adsorption must occur due to strong interactions with the adsorbent's surface. Furthermore, it was observed (data not shown) that loaded adsorbent particles exhibit a different

Table 6: Kinetic parameters obtained for intraparticle diffusion and Boyd models for adsorption of Ni(II) in the absence and presence of other metal ions.

		Ni	Ni + Cd	Ni + Cu	Ni + Pb
Intraparticle diffusion	$k_{P,1}$ 10^3 ($s^{-0.5}$)	1.8 ± 0.2	2.3 ± 0.2	1.1 ± 0.2	3.7 ± 0.1
	$A_{0,1}$	0.28 ± 0.01	0.22 ± 0.01	0.47 ± 0.03	0.15 ± 0.02
	R^2	0.9754	0.9860	0.9057	0.9961
	$k_{P,2}$ 10^3 ($s^{-0.5}$)	4.03 ± 0.07	3.9 ± 0.5	2.5 ± 0.1	—
	$A_{0,2}$	0.07 ± 0.01	0.10 ± 0.08	0.26 ± 0.02	—
	R^2	0.9994	0.9701	0.9968	—
Boyd	m 10^5 (s^{-1})	1.43 ± 0.02	1.7 ± 0.1	1.0 ± 0.3	3.5 ± 0.1
	y_0	0.106 ± 0.001	0.083 ± 0.007	0.34 ± 0.04	0.01 ± 0.01
	R^2	0.9991	0.9843	0.8625	0.9961

Table 7: Selectivity coefficients of the Schiff base-modified aerogel-like monolith.

Cation	$\alpha_{Cu,i}$	$\alpha_{Ni,i}$
Cd	3.7	9.4
Cu	1.0	1.8
Pb	7.5	5.4
Ni	0.6	1.0

color than pristine particles, which was shown to be associated with metal complexation [91]. Thus, we must conclude that the adsorption is due to complexation of cations by the Schiff base, which most likely occurs with partial loss of hydration water (chemisorption) [87].

We propose that the hemi-salen groups interact differently with the cations, due to the latter's hydrated radius (or its size relative to the distance between the electron donor atoms in the Schiff base) and the proximity of adjacent Schiff base groups. The imine and the hydroxyl group in the Schiff base are relatively close (distance estimated at 2.4 Å, Figure 7), compared to the cation's hydrated radius (3.9 Å in the equatorial direction of the Jahn-Teller distorted octahedron for copper, 4.1 Å for nickel, 4.6 Å for cadmium, and 5.1 Å for lead [110]). So, considering a single hemi-salen group, it is possible that the bigger cations are not complexed by both atoms, as they would retain a large radius even after partial loss of the hydration shell, and could be repelled by atoms neighboring the imine and hydroxyl groups. The Schiff base could then act as two different active sites, for cadmium and lead, resulting in a weaker interaction between the phases. This justifies the cadmium isotherm and the reduced removal of cadmium and lead. The Freundlich model fitted to the cadmium adsorption data the best, as a linear trend is observed. This shows that cadmium adsorption is due mainly to pore diffusion rather than interactions between solid and liquid phases. A different hypothesis, already mentioned, considers two adjacent hemi-salen groups complexing the metal together, in what would be a tetradentate salen ligand [46, 47, 49]. It is easily understandable that the distance between these groups will determine the cation size that acts as the coordination center. In this situation, potentially all the cations tested can be adsorbed, but because the distribution of the active sites in the adsorbent is not uniform, the distance between surface groups cannot be determined.

The removal observed is very reduced when compared to previous amine-modified aerogels [58] or mercapto-amine aerogels [80] but is higher than unmodified aerogels [58, 65]. The cumulative effect of the ionophore ligand, for which cation radius is important, and the impossibility of electrostatic interactions help to justify this observation. A silica aerogel not modified with Lewis bases is not a good heavy metal sorbent and only interacts with lead (the most labile) under the same conditions (uptake for copper of 2.5 mg g^{-1}, 15.7 mg g^{-1} for lead, 1.6 mg g^{-1} for cadmium, and 1.4 mg g^{-1} for nickel). The here presented Schiff base ORMOSIL aerogel-like monolith is much more efficient in nickel removal than the salen modified silica gel (uptake capacity of 4 mg g^{-1}) reported by Kursunlu et al. [53]. When modifying mesoporous silica with salen, Enache and coauthors found that the adsorption of lead increased a little (20% for MCM and up to 5% for HMS) up to 99 mg g^{-1} [52]. The adsorption of lead increased 49% with the incorporation of the salen reported in this work. The nickel uptake reported in this work is also superior to that of some amine-modified silicas (28 mg g^{-1}) [111] but is inferior to that of EDTA-modified silica (74 mg g^{-1}) [112] or poly (sodium 4-styrenesulfonate)-modified zeolitic imidazolate framework-8 (330 mg g^{-1}) [113]. The Schiff base silica aerogel-like monolith is a better nickel sorbent than natural minerals, zeolites, sawdust and biochar adsorbents [1, 114, 115], and other materials [116, 117].

3.4. Adsorption Kinetics and Selectivity. The HM adsorption by the prepared adsorbent was studied in binary mixtures, as a kinetic test. The total molar uptake results are presented in Table 4 and Figure 8. The kinetic curves for copper and nickel adsorption isolated and in binary mixtures are reported in Table 5 and Figure 9.

The plots from Figures 8 and 9 illustrate that a significant amount of adsorbates is adsorbed in a short period of time. From there on, the adsorption process continues slowly, which is more pronounced when nickel is present.

On the majority of datasets, the modified pseudo-second order kinetic model is reduced to pseudo-second order model, as there is no relevant initial adsorption. The fit quality criteria, AIC and BIC, agree that this model is clearly better than the pseudo-first order model, which indicates that the adsorption of the different sorbates is controlled by the surface reaction, i.e., the interaction with active surface sites. When an initial uptake is significant, AIC penalizes the modified pseudo-second order model for having more parameters (Tables 4 and 5) while BIC considers this model more adequate than the pseudo-first order one. Figures 8 and 9 clearly show that the kinetic data follows the pseudo-second order trend, and so this model was chosen as the most adequate. Figure 6 elucidates that, on the concentrations tested for the kinetic tests, we are near the BET curve knee, and thus, the insight provided by the kinetic tests does not allow to disprove the existence of multilayers since the BET theory assumes that the first layer is Langmuir-like, and so it is reduced to the Langmuir equation when there is only one adsorbed layer [70, 118].

Regarding the adsorption of nickel by the Schiff base-modified aerogel-like adsorbent, the analysis of Boyd model, considered for short adsorption times, shows that intraparticle diffusion is not the rate limiting step (Table 6). This was expected as the pseudo-second order fitted to the data, indicating that chemisorption is the limiting step. It should be noted that the pseudo-first order model, which was shown to be mathematically equivalent to the Boyd model derived for long adsorption times [119], did not fit well to the data. It can also be seen that, apart from nickel adsorption kinetics in the presence of lead, the adsorption process shows two linear regions, as described by Equation (9). The first stage involves a diffusion effect of the boundary layer, followed by a faster process which might be related with the interaction with the ionophore. For the case of Ni(II), in the presence of Pb(II), only one step is detected. Taking into account the magnitude of k_p, we may hypothesize that the boundary layer has no significant effect on the adsorption process.

When copper and nickel are mixed, the adsorption of copper (Figure 9(b)) is almost instantaneous and remains somewhat constant, while nickel adsorption increases over time and seems that it has not reached equilibrium after 24 hours (Figure 9(a)). Figure 8 shows that the mixtures of cadmium and lead with nickel have a higher uptake than those with copper. Figure 9 clarifies this observation by revealing that nickel adsorption is not affected by the presence of these interfering cations (considering the equilibrium uptakes and their experimental error in Table 5); hence, the equilibrium found has no statistically significant change for all situations presented, and its uptake is higher than that of copper. With copper (Figure 9(b)), interfering cations have a synergistic effect on the former's adsorption, enhancing it, and its equilibrium uptake is affected by the interferents.

The observation that nickel adsorption is unaffected by the presence of interferents is a clear indication of selectivity of the material towards this cation. Furthermore, this selectivity could not be achieved by mere nonspecific interactions between phases, meaning that the hemi-salen ligands in the aerogel-like monolith are strongly binding this cation, corroborating the idea of strong interactions for some cations. This is most likely the reason for the different shape of the nickel isotherm.

The recovery of nickel, achieved with the desorption tests with both desorption agents (HCl and HNO_3), was of 7%, meaning that the recovery of the adsorbed cation is not likely to be achieved without the degradation of the adsorbent as a consequence of strong adsorbent-adsorbate interactions. Thus, this is also an indication of the strong adsorption interaction between the cation and the adsorbent, in agreement with the chemisorption hypothesis drawn in the previous discussion.

The selectivity coefficients in the binary mixtures are reported in Table 7. The selectivity coefficients confirm that nickel is adsorbed preferentially, in the presence of the other tested cations, as expected. In the absence of nickel, a selectivity towards copper is verified as expected from salen ligands.

4. Conclusion

The preparation of a selective adsorbent for nickel was achieved by incorporating a salen ionophore in a silica network, resulting in a bright yellow adsorbent. The ORMOSIL aerogel-like monolith was dried via ambient pressure drying but remained a highly porous (85%) monolith, with a reduced linear shrinkage (10%). The small specific surface area obtained ($28\,m^2\,g^{-1}$) is typical for some modified silica aerogels and is a result of the macroporous structure of the material. The isotherm studies revealed that the BET curve models the adsorption of the majority of the tested cations, although different interactions with surface sites at higher sorbate concentrations seem more likely than the formation of multilayers. Nickel was the most adsorbed cation (experimental maximum of $50\,mg\,g^{-1}$), an improvement towards different reported materials. Kinetic studies evidenced a very fast initial uptake, which is sometimes reflected by what can be considered as an initial boost to the adsorption process that slows down as active sites become occupied. The adsorption of binary mixtures, not common in newly reported adsorbents, revealed a high affinity for both copper and nickel by the Schiff base-modified aerogel-like monolith. However, it is clear that copper is only the preferred sorbate in the absence of nickel, as copper uptake decreases slightly (in the presence of nickel) as time increases, and nickel uptake is not affected by the presence of other species in solution. The selectivity coefficients calculated indicate that the prepared adsorbent removes nickel ~9 times more than cadmium, ~5 times more than lead, and~ 2 times more than copper, confirming the fitness of this material for the separation of nickel from solutions with other metals. Further interfering ions should be tested in the future to assess the viability of the material here presented in separating nickel from complex mixtures/mixtures containing other common ions. The desorption of nickel was not very extensive, so further tests must be conducted in different conditions for the improvement of nickel release. Because of the high stability of Schiff base-nickel complex that was formed, desorption

might only be significant if ligands are used as desorption agents, and several ligands should be tested for this purpose. The economic value of nickel may trigger the interest in the new sorbent here developed, in particular due to its high selectivity, which can contribute to follow the circular economy concept. Additionally, these results pave the way for using silica-based aerogels as potential materials for acting as sensors of metal ions.

Data Availability

Data and material may be available upon request to the corresponding authors.

Conflicts of Interest

The authors declare that there is no conflict of interest regarding the publication of this article.

Acknowledgments

The authors acknowledge Pedro Maximiano for his cooperation with the computational calculus. J.P. Vareda acknowledges the PhD grant SFRH/BD/131280/2017 by *Fundação para a Ciência e a Tecnologia*, *I.P.* (FCT, Portugal) funded by national funds from MCTES (*Ministério da Ciência, Tecnologia e Ensino Superior*) and, when appropriate, cofunded by the European Commission through the European Social Fund. Consumables for the syntheses and characterizations performed at CIEPQPF and CQC research units were funded by national funds through the FCT and when appropriate cofunded by FEDER under the PT2020 Partnership Agreement under the projects POCI-01-0145-FEDER-006910 and POCI-01-0145-FEDER-007630 (FCT Refs. UIDB/EQU/00102/2020 and UIDB/QUI/00313/2020, respectively). Moreover, tests were also performed under the scope of the project "BIOSHELL" (Ref. "BLUEBIO/0003/2019–Recycling Crustaceans Shell Wastes for Developing Biodegradable Wastewater Cleaning Composites"), financed by FCT within program ERA-NET cofund on Blue Bioeconomy (BlueBio)—Unlocking the Potential of Aquatic Bioresources.

References

[1] J. P. Vareda, A. J. M. Valente, and L. Durães, "Assessment of heavy metal pollution from anthropogenic activities and remediation strategies: a review," *Journal of Environmental Management*, vol. 246, pp. 101–118, 2019.

[2] D. C. Adriano, *Trace elements in terrestrial environments: biogeochemistry, bioavailability, and risks of metals*, Springer, 2nd edition, 2001.

[3] J. H. Park, G. K. Choppala, N. S. Bolan, J. W. Chung, and T. Chuasavathi, "Biochar reduces the bioavailability and phytotoxicity of heavy metals," *Plant and Soil*, vol. 348, no. 1-2, pp. 439–451, 2011.

[4] N. Bolan, A. Kunhikrishnan, R. Thangarajan et al., "Remediation of heavy metal(loid)s contaminated soils - To mobilize or to immobilize?," *Journal of Hazardous Materials*, vol. 266, pp. 141–166, 2014.

[5] A. Kabata-Pendias, *Trace Elements in Soils and Plants*, CRC Press, USA, 4th edition, 2011.

[6] D. C. Adriano, W. W. Wenzel, J. Vangronsveld, and N. S. Bolan, "Role of assisted natural remediation in environmental cleanup," *Geoderma*, vol. 122, no. 2-4, pp. 121–142, 2004.

[7] P.-A. Amundsen, F. J. Staldvik, A. A. Lukin, N. A. Kashulin, O. A. Popova, and Y. S. Reshetnikov, "Heavy metal contamination in freshwater fish from the border region between Norway and Russia," *Science of the Total Environment*, vol. 201, no. 3, pp. 211–224, 1997.

[8] C. Guerreiro, A. G. Ortiz, F. de Leeuw, M. Viana, and J. Horálek, *Air Quality in Europe — 2016 Report*, European Environment Agency, Denmark, 2016.

[9] The International Council on Mining and Metals, *Trends in the Mining and Metals Industry in Mining's Contribution to Sustainable Development: the series*, 2012.

[10] World Bank Group, *Commodity Markets Outlook January*, Washington, 2017.

[11] C. P. Cutler, "Use of metals in our society," in *Metal Allergy: From Dermatitis to Implant and Device Failure*, J. K. Chen and J. P. Thyssen, Eds., pp. 3–16, Springer International Publishing, Cham, 2018.

[12] European Environment Agency, "Indicator assessment: heavy metal emissions," in *EEA Indicators*, Denmark, 2019.

[13] K. Oorts, "Copper," in *Heavy Metals in Soils: Trace Metals and Metalloids in Soils and their Bioavailability*, J. B. Alloway, Ed., pp. 367–394, Springer, Dordrecht, 2013.

[14] B. J. Alloway, "Introduction," in *Heavy Metals in Soils: Trace Metals and Metalloids in Soils and their Bioavailability*, B. J. Alloway, Ed., pp. 3–9, Springer, Netherlands: Dordrecht, 2013.

[15] J. Clavadetscher, S. Hoffmann, A. Lilienkampf et al., "Copper catalysis in living systems and in situ drug synthesis," *Angewandte Chemie International Edition*, vol. 55, no. 50, pp. 15662–15666, 2016.

[16] L. Su, J. Dong, L. Liu et al., "Copper catalysis for selective heterocoupling of terminal alkynes," *Journal of the American Chemical Society*, vol. 138, no. 38, pp. 12348–12351, 2016.

[17] F. Lang, D. Zewge, I. N. Houpis, and R. P. Volante, "Amination of aryl halides using copper catalysis," *Tetrahedron Letters*, vol. 42, no. 19, pp. 3251–3254, 2001.

[18] E. Steinnes, "Lead," in *Heavy Metals in Soils: Trace Metals and Metalloids in Soils and their Bioavailability*, J. B. Alloway, Ed., pp. 395–409, Springer, Dordrecht, 2013.

[19] European Chemicals Agency, "Lead in shot, bullets and fishing weights 2019," April 2021, https://echa.europa.eu/hot-topics/lead-in-shot-bullets-and-fishing-weights.

[20] S. Das, "3 - Review of restricted substances in apparel," in *Product Safety and Restricted Substances in Apparel*, S. Das, Ed., pp. 14–28, Woodhead Publishing, India, 2013.

[21] Occupational Safety & Health Administration, "Cadmium," April 2021, https://www.osha.gov/cadmium.

[22] European Chemicals Agency, "Substances restricted under REACH 2021," April 2021, https://echa.europa.eu/substances-restricted-under-reach.

[23] S. Z. Tasker, E. A. Standley, and T. F. Jamison, "Recent advances in homogeneous nickel catalysis," *Nature*, vol. 509, no. 7500, pp. 299–309, 2014.

[24] World Bank Group, *Commodity Markets Outlook April*, Washington, 2020.

[25] A. Duda-Chodak and U. Blaszczyk, "The impact of nickel on human health," *Journal of Elementology*, vol. 13, no. 4, pp. 685–696, 2008.

[26] C. Gonnelli and G. Renella, "Chromium and Nickel," in *Heavy Metals in Soils: Trace Metals and Metalloids in Soils and their Bioavailability*, J. B. Alloway, Ed., pp. 313–333, Springer, Dordrecht, 2013.

[27] F. Fu and Q. Wang, "Removal of heavy metal ions from wastewaters: a review," *Journal of Environmental Management*, vol. 92, no. 3, pp. 407–418, 2011.

[28] T. A. Kurniawan, G. Y. S. Chan, W.-H. Lo, and S. Babel, "Physico-chemical treatment techniques for wastewater laden with heavy metals," *Chemical Engineering Journal*, vol. 118, no. 1-2, pp. 83–98, 2006.

[29] A. Dąbrowski, Z. Hubicki, P. Podkościelny, and E. Robens, "Selective removal of the heavy metal ions from waters and industrial wastewaters by ion-exchange method," *Chemosphere*, vol. 56, no. 2, pp. 91–106, 2004.

[30] A. Heidari, H. Younesi, Z. Mehraban, and H. Heikkinen, "Selective adsorption of Pb(II), Cd(II), and Ni(II) ions from aqueous solution using chitosan-MAA nanoparticles," *International Journal of Biological Macromolecules*, vol. 61, pp. 251–263, 2013.

[31] S. M. Shaheen, A. S. Derbalah, and F. S. Moghanm, "Removal of heavy metals from aqueous solution by zeolite in competitive sorption system," *International Journal of Environmental Science and Development*, vol. 3, no. 4, pp. 362–367, 2012.

[32] P. D. Verweij, T. Dugué, W. L. Driessen, J. Reedijk, B. Rowatt, and D. C. Sherrington, "Metal uptake by N,N′-bis(2-benzimidazolylmethyl) amine immobilized on poly(glycidyl methacrylate-co-ethylene glycol dimethacrylate)," *Reactive Polymers*, vol. 14, no. 3, pp. 213–227, 1991.

[33] H. A. Dam and D. Kim, "Selective copper(II) sorption behavior of surface-imprinted core–shell-type polymethacrylate microspheres," *Industrial & Engineering Chemistry Research*, vol. 48, no. 12, pp. 5679–5685, 2009.

[34] V. Dudler, L. F. Lindoy, D. Sallin, and C. W. Schlaepfer, "An oxygen-nitrogen donor macrocycle immobilized on silica gel. A reagent showing high selectivity for copper(II) in the presence of cobalt (II), nickel (II), zinc (II) or cadmium (II)," *Australian Journal of Chemistry*, vol. 40, no. 9, pp. 1557–1563, 1987.

[35] A. Nosrati, M. Larsson, J. B. Lindén, Z. Zihao, J. Addai-Mensah, and M. Nydén, "Polyethyleneimine functionalized mesoporous diatomite particles for selective copper recovery from aqueous media," *International Journal of Mineral Processing*, vol. 166, pp. 29–36, 2017.

[36] A. El Hanandeh, Z. Mahdi, and M. S. Imtiaz, "Modelling of the adsorption of Pb, Cu and Ni ions from single and multi-component aqueous solutions by date seed derived biochar: comparison of six machine learning approaches," *Environmental Research*, vol. 192, article 110338, 2021.

[37] S. A. Al-Saydeh, M. H. El-Naas, and S. J. Zaidi, "Copper removal from industrial wastewater: a comprehensive review," *Journal of Industrial and Engineering Chemistry*, vol. 56, pp. 35–44, 2017.

[38] J. P. Vareda, A. J. M. Valente, and L. Durães, "Ligands as copper and nickel ionophores: applications and implications on wastewater treatment," *Advances in Colloid and Interface Science*, vol. 289, article 102364, 2021.

[39] R. Hernández-Molina and A. Mederos, "1.19 - Acyclic and Macrocyclic Schiff Base Ligands," in *Comprehensive Coordination Chemistry II*, J. A. McCleverty and T. J. Meyer, Eds., pp. 411–446, Pergamon, Oxford, 2003.

[40] D. Peralta-Domínguez, M. Rodríguez, G. Ramos-Ortíz et al., "A Schiff base derivative from cinnamaldehyde for colorimetric detection of Ni^{2+} in water," *Sensors and Actuators B: Chemical*, vol. 207, pp. 511–517, 2015.

[41] S. Goswami, S. Chakraborty, S. Paul, S. Halder, and A. C. Maity, "A simple quinoxaline-based highly sensitive colorimetric and ratiometric sensor, selective for nickel and effective in very high dilution," *Tetrahedron Letters*, vol. 54, no. 37, pp. 5075–5077, 2013.

[42] J. H. Kang, S. Y. Lee, H. M. Ahn, and C. Kim, "A novel colorimetric chemosensor for the sequential detection of Ni^{2+} and CN^{-} in aqueous solution," *Sensors and Actuators B: Chemical*, vol. 242, pp. 25–34, 2017.

[43] M. R. Ganjali, M. Hosseini, M. Motalebi et al., "Selective recognition of Ni^{2+} ion based on fluorescence enhancement chemosensor," *Spectrochimica Acta Part A: Molecular and Biomolecular Spectroscopy*, vol. 140, pp. 283–287, 2015.

[44] V. K. Gupta, A. K. Singh, and M. K. Pal, "Ni(II) selective sensors based on Schiff bases membranes in poly(vinyl chloride)," *Analytica Chimica Acta*, vol. 624, no. 2, pp. 223–231, 2008.

[45] V. K. Gupta, A. K. Jain, Z. Ishtaiwi, H. Lang, and G. Maheshwari, "Ni^{2+} selective sensors based on meso-tetrakis-{4-[tris-(4-allyl dimethylsilyl-phenyl)-silyl]-phenyl}porphyrin and $(sal)_2$trien in poly(vinyl chloride) matrix," *Talanta*, vol. 73, no. 5, pp. 803–811, 2007.

[46] R. Antony, R. Marimuthu, P. Vishnoi, and R. Murugavel, "Ethoxysilane appended M(II) complexes and their SiO_2/MCM-41 supported forms as catalysts for efficient oxidation of secondary alcohols," *Inorganica Chimica Acta*, vol. 469, pp. 173–182, 2018.

[47] S. Bhunia and S. Koner, "Tethering of nickel(II) Schiff-base complex onto mesoporous silica: an efficient heterogeneous catalyst for epoxidation of olefins," *Polyhedron*, vol. 30, no. 11, pp. 1857–1864, 2011.

[48] K. M. Parida, S. Singha, and P. C. Sahoo, "A facile method for promoting activities of vanadium–Schiffbase complex anchored on organically modified MCM-41 in epoxidation reaction," *Journal of Molecular Catalysis A: Chemical*, vol. 325, no. 1-2, pp. 40–47, 2010.

[49] M. Nikoorazm, A. Ghorbani-Choghamarani, H. Mahdavi, and S. M. Esmaeili, "Efficient oxidative coupling of thiols and oxidation of sulfides using UHP in the presence of Ni or Cd salen complexes immobilized on MCM-41 mesoporous as novel and recoverable nanocatalysts," *Microporous and Mesoporous Materials*, vol. 211, pp. 174–181, 2015.

[50] Y. Yang, Y. Zhang, S. Hao et al., "Heterogenization of functionalized cu(II) and VO(IV) Schiff base complexes by direct immobilization onto amino-modified SBA-15: styrene oxidation catalysts with enhanced reactivity," *Applied Catalysis A: General*, vol. 381, no. 1-2, pp. 274–281, 2010.

[51] Y. Yang, Y. Zhang, S. Hao, and Q. Kan, "Tethering of Cu(II), Co(II) and Fe(III) tetrahydro-salen and salen complexes onto amino-functionalized SBA-15: effects of salen ligand hydrogenation on catalytic performances for aerobic epoxidation of styrene," *Chemical Engineering Journal*, vol. 171, no. 3, pp. 1356–1366, 2011.

[52] D. F. Enache, E. Vasile, C. M. Simonescu et al., "Schiff base-functionalized mesoporous silicas (MCM-41, HMS) as Pb(ii) adsorbents," *RSC Advances*, vol. 8, no. 1, pp. 176–189, 2018.

[53] A. N. Kursunlu, E. Guler, H. Dumrul, O. Kocyigit, and I. H. Gubbuk, "Chemical modification of silica gel with synthesized new Schiff base derivatives and sorption studies of cobalt (II) and nickel (II)," *Applied Surface Science*, vol. 255, no. 21, pp. 8798–8803, 2009.

[54] W. Qiao, P. Zhang, L. Sun et al., "Adsorption performance and mechanism of Schiff base functionalized polyamidoamine dendrimer/silica for aqueous Mn(II) and Co(II)," *Chinese Chemical Letters*, vol. 31, no. 10, pp. 2742–2746, 2020.

[55] B. Mondal, S. Lohar, S. Pal, A. Maji, and P. Chattopadhyay, "A new chemosensor selective for Cu^{2+} ions through fluorescence quenching approach applicable to real samples," *Journal of the Indian Chemical Society*, vol. 92, pp. 1–8, 2015.

[56] M. B. Gholivand, P. Niroomandi, A. Yari, and M. Joshagani, "Characterization of an optical copper sensor based on N,N′-bis(salycilidene)-1,2-phenylenediamine," *Analytica Chimica Acta*, vol. 538, no. 1-2, pp. 225–231, 2005.

[57] J. P. Vareda and L. Durães, "Functionalized silica xerogels for adsorption of heavy metals from groundwater and soils," *Journal of Sol-Gel Science and Technology*, vol. 84, no. 3, pp. 400–408, 2017.

[58] J. P. Vareda, A. J. M. Valente, and L. Durães, "Silica aerogels/xerogels modified with nitrogen-containing groups for heavy metal adsorption," *Molecules*, vol. 25, no. 12, p. 2788, 2020.

[59] J. P. Vareda, T. Matias, and L. Durães, "Facile preparation of ambient pressure dried aerogel-like monoliths with reduced shrinkage based on vinyl-modified silica networks," *Ceramics International*, vol. 44, no. 14, pp. 17453–17458, 2018.

[60] A. G. Howard and N. H. Khdary, "Spectrofluorimetric determination of surface-bound thiol groups and its application to the analysis of thiol-modified silicas," *Analyst*, vol. 129, no. 9, pp. 860–863, 2004.

[61] H.-S. Jung, D.-S. Moon, and J.-K. Lee, "Quantitative analysis and efficient surface modification of silica nanoparticles," *Journal of Nanomaterials*, vol. 2012, Article ID 593471, 8 pages, 2012.

[62] T. D. Kühne, M. Iannuzzi, M. Del Ben et al., "CP2K: an electronic structure and molecular dynamics software package - quickstep: efficient and accurate electronic structure calculations," *The Journal of Chemical Physics*, vol. 152, no. 19, article 194103, 2020.

[63] S. Grimme, C. Bannwarth, and P. Shushkov, "A robust and accurate tight-binding quantum chemical method for structures, vibrational frequencies, and noncovalent interactions of large molecular systems parametrized for all spd-block elements (Z = 1–86)," *Journal of Chemical Theory and Computation*, vol. 13, no. 5, pp. 1989–2009, 2017.

[64] S. Grimme, J. Antony, S. Ehrlich, and H. Krieg, "A consistent and accurate ab initio parametrization of density functional dispersion correction (DFT-D) for the 94 elements H-Pu," *The Journal of Chemical Physics*, vol. 132, no. 15, article 154104, 2010.

[65] A. Lamy-Mendes, R. B. Torres, J. P. Vareda et al., "Amine modification of silica aerogels/xerogels for removal of relevant environmental pollutants," *Molecules*, vol. 24, no. 20, p. 3701, 2019.

[66] D. Posada and T. R. Buckley, "Model selection and model averaging in phylogenetics: advantages of Akaike information criterion and Bayesian approaches over likelihood ratio tests," *Systematic Biology*, vol. 53, no. 5, pp. 793–808, 2004.

[67] H. M. F. Freundlich, "Over the adsorption in solution," *The Journal of Physical Chemistry*, vol. 57, pp. 385–471, 1906.

[68] K. Y. Foo and B. H. Hameed, "Insights into the modeling of adsorption isotherm systems," *Chemical Engineering Journal*, vol. 156, no. 1, pp. 2–10, 2010.

[69] S. Brunauer, P. H. Emmett, and E. Teller, "Adsorption of gases in multimolecular layers," *Journal of the American Chemical Society*, vol. 60, no. 2, pp. 309–319, 1938.

[70] A. Ebadi, J. S. Soltan Mohammadzadeh, and A. Khudiev, "What is the correct form of BET isotherm for modeling liquid phase adsorption?," *Adsorption*, vol. 15, no. 1, pp. 65–73, 2009.

[71] T. D. Naylor, "20 - Permeation Properties A2 - Allen, Geoffrey," in *Comprehensive Polymer Science and Supplements*, J. C. Bevington, Ed., pp. 643–668, Pergamon, Amsterdam, 1989.

[72] S. Lagergreen, "Zur theorie der sogenannten adsorption gelöster stoffe," *Zeitschrift für Chemie und Industrie der Kolloide*, vol. 2, no. 1, pp. 15–15, 1907.

[73] Y. S. Ho and G. McKay, "Sorption of dye from aqueous solution by peat," *Chemical Engineering Journal*, vol. 70, no. 2, pp. 115–124, 1998.

[74] F.-C. Wu, R.-L. Tseng, and R.-S. Juang, "Initial behavior of intraparticle diffusion model used in the description of adsorption kinetics," *Chemical Engineering Journal*, vol. 153, no. 1–3, pp. 1–8, 2009.

[75] H. Qiu, L. Lv, B. C. Pan, Q. J. Zhang, W. M. Zhang, and Q. X. Zhang, "Critical review in adsorption kinetic models," *Journal of Zhejiang University Science A*, vol. 10, no. 5, pp. 716–724, 2009.

[76] H.-T. Fan, W. Sun, B. Jiang et al., "Adsorption of antimony(III) from aqueous solution by mercapto-functionalized silica-supported organic-inorganic hybrid sorbent: mechanism insights," *Chemical Engineering Journal*, vol. 286, pp. 128–138, 2016.

[77] K. V. Kumar and K. Porkodi, "Mass transfer, kinetics and equilibrium studies for the biosorption of methylene blue using Paspalum notatum," *Journal of Hazardous Materials*, vol. 146, no. 1-2, pp. 214–226, 2007.

[78] J. P. Vareda, P. Maximiano, L. P. Cunha, A. F. Ferreira, P. N. Simões, and L. Durães, "Effect of different types of surfactants on the microstructure of methyltrimethoxysilane-derived silica aerogels: a combined experimental and computational approach," *Journal of Colloid and Interface Science*, vol. 512, pp. 64–76, 2018.

[79] J. P. Vareda, A. Lamy-Mendes, and L. Durães, "A reconsideration on the definition of the term aerogel based on current drying trends," *Microporous and Mesoporous Materials*, vol. 258, Supplement C, pp. 211–216, 2018.

[80] J. P. Vareda and L. Durães, "Efficient adsorption of multiple heavy metals with tailored silica aerogel-like materials," *Environmental Technology*, vol. 40, no. 4, pp. 529–541, 2019.

[81] N. Leventis, A. Sadekar, N. Chandrasekaran, and C. Sotiriou-Leventis, "Click synthesis of monolithic silicon carbide aerogels from polyacrylonitrile-coated 3D silica networks," *Chemistry of Materials*, vol. 22, no. 9, pp. 2790–2803, 2010.

[82] S. S. Kistler, "Coherent expanded aerogels and jellies," *Nature*, vol. 127, no. 3211, p. 741, 1931.

[83] N. Hüsing and U. Schubert, "Aerogels," in *Ullmann's Encyclopedia of Industrial Chemistry*, C. Ley, Ed., Wiley-VCH Verlag GmbH & Co. KGaA, 2000.

[84] E. Soto-Cantu, R. Cueto, J. Koch, and P. S. Russo, "Synthesis and rapid characterization of amine-functionalized silica," *Langmuir*, vol. 28, no. 13, pp. 5562–5569, 2012.

[85] W. Sheng, W. Wei, J. Li et al., "Amine-functionalized magnetic mesoporous silica nanoparticles for DNA separation," *Applied Surface Science*, vol. 387, pp. 1116–1124, 2016.

[86] I. L. Hsiao, S. Fritsch-Decker, A. Leidner et al., "Biocompatibility of amine-functionalized silica nanoparticles: the role of surface coverage," *Small*, vol. 15, no. 10, p. 1805400, 2019.

[87] H. Bradl, C. Kim, U. Kramar, and D. StÜben, "Chapter 2 Interactions of Heavy Metals," in *Interaction and Remediation*, H. B. Bradl, Ed., vol. 6, pp. 28–164, 2005.

[88] M. Thommes, K. Kaneko, A. V. Neimark et al., "Physisorption of gases, with special reference to the evaluation of surface area and pore size distribution (IUPAC Technical Report)," *Pure and Applied Chemistry*, vol. 87, no. 9-10, pp. 1051–1069, 2015.

[89] J. S. Piccin, T. R. S. A. Cadaval, L. A. A. de Pinto, and G. L. Dotto, "Adsorption Isotherms in Liquid Phase: Experimental, Modeling, and Interpretations," in *Adsorption Processes for Water Treatment and Purification*, A. Bonilla-Petriciolet, D. I. Mendoza-Castillo, and H. E. Reynel-Ávila, Eds., pp. 19–51, Springer International Publishing, Cham, 2017.

[90] X. Cao, L. Ma, B. Gao, and W. Harris, "Dairy-manure derived biochar effectively sorbs lead and atrazine," *Environmental Science & Technology*, vol. 43, no. 9, pp. 3285–3291, 2009.

[91] A. Benhamou, M. Baudu, Z. Derriche, and J. P. Basly, "Aqueous heavy metals removal on amine-functionalized Si-MCM-41 and Si-MCM-48," *Journal of Hazardous Materials*, vol. 171, no. 1-3, pp. 1001–1008, 2009.

[92] L. Bois, A. Bonhommé, A. Ribes, B. Pais, G. Raffin, and F. Tessier, "Functionalized silica for heavy metal ions adsorption," *Colloids and Surfaces A: Physicochemical and Engineering Aspects*, vol. 221, no. 1-3, pp. 221–230, 2003.

[93] Q. Cheng, Q. Huang, S. Khan et al., "Adsorption of Cd by peanut husks and peanut husk biochar from aqueous solutions," *Ecological Engineering*, vol. 87, Supplement C, pp. 240–245, 2016.

[94] J. Deng, Y. Liu, S. Liu et al., "Competitive adsorption of Pb(II), Cd(II) and Cu(II) onto chitosan-pyromellitic dianhydride modified biochar," *Journal of Colloid and Interface Science*, vol. 506, Supplement C, pp. 355–364, 2017.

[95] A. M. F. Guimarães, V. S. T. Ciminelli, and W. L. Vasconcelos, "Smectite organofunctionalized with thiol groups for adsorption of heavy metal ions," *Applied Clay Science*, vol. 42, no. 3-4, pp. 410–414, 2009.

[96] X. Liang, Y. Xu, G. Sun, L. Wang, Y. Sun, and X. Qin, "Preparation, characterization of thiol-functionalized silica and application for sorption of Pb^{2+} and Cd^{2+}," *Colloids and Surfaces A: Physicochemical and Engineering Aspects*, vol. 349, no. 1-3, pp. 61–68, 2009.

[97] S. Wu, F. Li, R. Xu, S. Wei, and G. Li, "Synthesis of thiol-functionalized MCM-41 mesoporous silicas and its application in Cu(II), Pb(II), Ag(I), and Cr(III) removal," *Journal of Nanoparticle Research*, vol. 12, no. 6, pp. 2111–2124, 2010.

[98] F. Wang, Y. Pan, P. Cai, T. Guo, and H. Xiao, "Single and binary adsorption of heavy metal ions from aqueous solutions using sugarcane cellulose-based adsorbent," *Bioresource Technology*, vol. 241, Supplement C, pp. 482–490, 2017.

[99] S. Prakash, M. Kumar, B. P. Tripathi, and V. K. Shahi, "Sol–gel derived poly(vinyl alcohol)-3-(2-aminoethylamino) propyl trimethoxysilane: cross-linked organic–inorganic hybrid beads for the removal of Pb(II) from aqueous solution," *Chemical Engineering Journal*, vol. 162, no. 1, pp. 28–36, 2010.

[100] A. M. Kłonkowski, B. Grobelna, T. Widernik, A. Jankowska-Frydel, and W. Mozgawa, "The coordination state of copper(II) complexes anchored and grafted onto the surface of organically modified silicates," *Langmuir*, vol. 15, no. 18, pp. 5814–5819, 1999.

[101] M. Sćiban, B. Radetić, Z. Kevresan, and M. Klasnja, "Adsorption of heavy metals from electroplating wastewater by wood sawdust," *Bioresource Technology*, vol. 98, no. 2, pp. 402–409, 2007.

[102] Y. H. Teow, L. M. Kam, and A. W. Mohammad, "Synthesis of cellulose hydrogel for copper (II) ions adsorption," *Journal of Environmental Chemical Engineering*, vol. 6, no. 4, pp. 4588–4597, 2018.

[103] N. Danesh, M. Ghorbani, and A. Marjani, "Separation of copper ions by nanocomposites using adsorption process," *Scientific Reports*, vol. 11, no. 1, p. 1676, 2021.

[104] S. Batool, M. Idrees, Q. Hussain, and J. Kong, "Adsorption of copper (II) by using derived-farmyard and poultry manure biochars: efficiency and mechanism," *Chemical Physics Letters*, vol. 689, pp. 190–198, 2017.

[105] K. F. Lam, X. Chen, G. McKay, and K. L. Yeung, "Anion effect on Cu^{2+} adsorption on NH_2-MCM-41," *Industrial & Engineering Chemistry Research*, vol. 47, no. 23, pp. 9376–9383, 2008.

[106] A. d. O. Jorgetto, A. C. P. da Silva, M. H. P. Wondracek et al., "Multilayer adsorption of Cu(II) and Cd(II) over Brazilian Orchid Tree (*Pata- de-vaca*) and its adsorptive properties," *Applied Surface Science*, vol. 345, pp. 81–89, 2015.

[107] M. M. Bhadbhade and D. Srinivas, "Effects on molecular association, chelate conformation, and reactivity toward substitution in copper Cu(5-X-salen) complexes, salen2- = N,N'-ethylenebis(salicylidenaminato), X = H, CH3O, and Cl: synthesis, x-ray structures, and EPR investigations," *Inorganic Chemistry*, vol. 32, no. 24, pp. 5458–5466, 1993.

[108] M. Mohammadikish and F. Bagheri, "Synthesis and characterization of [Cu(salen)]2 coordination nano-assembly by a green and simple method," *Zeitschrift für Kristallographie - Crystalline Materials*, vol. 232, no. 6, pp. 407–414, 2017.

[109] H. Dong, W. Tao, J. Bi et al., "Self-assembly of copper and cobalt complexes with hierarchical size and catalytic properties for hydroxylation of phenol," *Nanoscale Research Letters*, vol. 6, no. 1, p. 484, 2011.

[110] I. Persson, "Hydrated metal ions in aqueous solution: how regular are their structures?," *Pure and Applied Chemistry*, vol. 82, no. 10, pp. 1901–1917, 2010.

[111] H. Faghihian, H. Nourmoradi, and M. Shokouhi, "Removal of copper (II) and nickel (II) from aqueous media using silica aerogel modified with amino propyl triethoxysilane as an adsorbent: equilibrium, kinetic, and isotherms study," *Desalination and Water Treatment*, vol. 52, no. 1-3, pp. 305–313, 2013.

[112] R. Kumar, M. A. Barakat, Y. A. Daza, H. L. Woodcock, and J. N. Kuhn, "EDTA functionalized silica for removal of Cu(II), Zn(II) and Ni(II) from aqueous solution," *Journal of Colloid and Interface Science*, vol. 408, pp. 200–205, 2013.

[113] C. Ji, J. Zhang, R. Jia, W. Zhang, L. Lv, and B. Pan, "Sorption enhancement of nickel(II) from wastewater by ZIF-8

modified with poly (sodium 4-styrenesulfonate): mechanism and kinetic study," *Chemical Engineering Journal*, vol. 414, article 128812, 2021.

[114] L. Yang, L. He, J. Xue et al., "Highly efficient nickel (II) removal by sewage sludge biochar supported α-Fe_2O_3 and α-FeOOH: sorption characteristics and mechanisms," *PLoS One*, vol. 14, no. 6, article e0218114, 2019.

[115] M. Šuránek, Z. Melichová, V. Kureková, L. Kljajević, and S. Nenadović, "Removal of nickel from aqueous solutions by natural bentonites from Slovakia," *Materials*, vol. 14, no. 2, p. 282, 2021.

[116] M. N. Siddiqui, I. Ali, M. Asim, and B. Chanbasha, "Quick removal of nickel metal ions in water using asphalt-based porous carbon," *Journal of Molecular Liquids*, vol. 308, article 113078, 2020.

[117] D. M. Veneu, L. Yokoyama, O. G. C. Cunha, C. L. Schneider, and M. B. . M. Monte, "Nickel sorption using bioclastic granules as a sorbent material: equilibrium, kinetic and characterization studies," *Journal of Materials Research and Technology*, vol. 8, no. 1, pp. 840–852, 2019.

[118] K. D. Hammond and W. C. Conner, "Chapter One - Analysis of Catalyst Surface Structure by Physical Sorption," in *Advances in Catalysis*, B. C. Gates and F. C. Jentoft, Eds., pp. 1–101, Academic Press, 2013.

[119] W. Plazinski and W. Rudzinski, "Kinetics of adsorption at solid/solution interfaces controlled by intraparticle diffusion: a theoretical analysis," *The Journal of Physical Chemistry C*, vol. 113, no. 28, pp. 12495–12501, 2009.